The gut contractile organoid: a novel model for studying the gut motility regulated by coordinating signals between interstitial cells of Cajal and smooth muscles

Rei Yagasaki[1,2], Ryo Nakamura[1,3], Yuuki Shikaya[1,4], Ryosuke Tadokoro[1,5], Ruolin Hao[6,7], Zhe Wang[6,7], Mototsugu Eiraku[6,7], Masafumi Inaba[1] and Yoshiko Takahashi[1,8]

1: Department of Zoology, Graduate School of Science, Kyoto University Sakyo-ku, Kyoto 606-8502, Japan
2: Present Address: WPI Nano Life Science Institute (WPI-NanoLSI), Kanazawa University, Kakuma-machi, Kanazawa 920-1192, Japan
3: Present Address: Ushimado Marine Institute, Okayama University, Setouchi, Okayama 701-4303, Japan
4: Present Address: Sorbonne Université, CNRS, Institut de la Mer de Villefranche, UMR7009 Laboratoire de Biologie du Développement de Villefranche-sur-Mer (LBDV), Villefranche-sur-Mer, France
5: Present Address: Department of Bioscience, Okayama University of Science, Okayama, Japan
6: Institute for Life and Medical Sciences, Kyoto University, Sakyo-ku, Kyoto 606-8507, Japan
7: Department of Polymer Chemistry, Graduate School of Engineering, Kyoto University, Kyoto 615-8510, Japan
8: Author to whom all correspondence should be addressed.
email: yotayota@develop.zool.kyoto-u.ac.jp

Keywords:
gut contraction, interstitial cells of Cajal, smooth muscle cells, organoid, gap junction

Abstract

The gut undergoes peristaltic movements regulated by intricate cellular interactions. However, they have poorly been explored due to a lack of model system. We here developed a novel contractile organoid that is derived from the muscle layer of chicken embryonic hindgut. The organoid contained smooth muscle cells (SMCs) and interstitial cells of Cajal (ICCs; pacemaker) with few enteric neurons, and underwent periodic contractions. The organoid formed by self-organization with morphological arrangements of ICCs (internal) and SMCs (peripheral), allowing identification of these cells in live. GCaMP-Ca^{2+} imaging analyses revealed that Ca^{2+} transients between ICC-ICC, SMC-SMC or SMC-ICC were markedly coordinated. Pharmacological studies further showed that gap junctions play a role in ICC-to-SMC signaling, and also possible feedback from SMC's contraction to ICC's pace-making activities. In addition, two organoids with different rhythm became synchronized when mediated by SMCs, unveiling a novel contribution of SMCs to ICC's pace-making. The gut contractile organoid developed in this study offers a useful model to understand the mechanisms underlying the rhythm coordination between/among ICCs and SMCs during gut peristaltic movements.

Introduction

In the gut, ingested material is conveyed properly along the gut axis by the gut movements called peristalsis, which is recognized as wave-like propagation of a local constriction. The physiology of gut peristalsis has extensively been studied in adults, where the peristalsis plays pivotal roles in effective transportation and digestion/absorption of inter-luminal contents. And many cases of gut-related pathology are associated with peristaltic disfunctions. The gut peristaltic movements are achieved by intricate regulations of intercellular functions among multiple cell types. At the site of origin of peristaltic waves (OPW), a local constriction emerges along the circumferential axis, and this is soon followed by a progressive wave of the contraction along the gut axis. During these processes, the circumferential constriction demands multiple SMCs to achieve simultaneous contraction. However, due to the complex structure of the gut, how such synchronization/coordination in SMCs is regulated remains largely undetermined.

It is known in vertebrates that the embryonic gut undergoes peristaltic movements even without experience of food intake. The embryonic gut therefore serves as a powerful model to study the intrinsic mechanisms underlying the peristalsis contrasting with the adult gut where ingested content influences the gut motility increasing complexity in analyses. We have recently reported using chicken embryos that sites of OPW are randomly distributed along the gut axis at early stages, and they later become confined to specific sites, and this confinement of OPWs enables rhythmic and patterned peristaltic movements (Shikaya et al., 2022). One of the long-standing and important questions is how the synchronized/coordinated contraction is achieved.

In a long history of gut motility studies, it has been known that enteric nervous system (ENS), smooth muscle cells (SMCs) and interstitial cells of Cajal (ICCs) play important roles in peristaltic movements (Barajas-Lopez et al., 1989; Camborova et al., 2003; Chevalier et al., 2020; Huizinga et al., 1995; Kito et al., 2005; Liu et al., 1998; Rumessen & Thuneberg, 1996; Sanders et al., 1991; Takaki, 2003; Takayama et al., 2002; Thomsen et al., 1998). It has widely been accepted that: 1) at early embryonic stages, gut movement/peristalsis does not require ENS activity, 2) ICCs serve as a pacemaker dictating their rhythm to SMCs, 3) the contraction is executed by SMC and not by ICCs, since thick fibers of myosin are found solely in SMCs. A series of elaborate electrophysiological studies showed that slow waves (a type of changes in membrane potential characteristic of gut movements) occur intrinsically in ICCs but not in SMCs, and that these slow waves lead to voltage-dependent Ca^{2+} influx evoking action potential, which is somehow transmitted to SMCs to execute gut contraction in register with ICC's pace-making rhythm (Baker et al., 2021; Torihashi et al., 2002). The knowledge that ICCs

85 act as a pacemaker was supported by compelling evidence obtained by c-Kit-deficient
86 mouse mutants (W/W^v), in which ICC differentiation was severely affected leading to a
87 failure of gut peristalsis (Huizinga et al., 1995; Torihashi et al., 1999). However, it
88 remains largely unexplored how the intrinsic/spontaneous rhythm in a single ICC
89 becomes synchronized among multiple ICCs which constitute intricate networks in the
90 gut. It has also been under debate to what extend the gap junction contributes to cell-cell
91 communications between ICCs, SMCs or ICC-SMC. One reason is that it has been
92 difficult to stably maintain SMCs and ICCs in cell culture condition, and also to
93 distinguish ICCs from SMCs in the living gut (these two types of cells originate from the
94 same progenitors of splanchnopleural mesoderm during development). Thus, a novel
95 model system has been awaited to circumvent these obstacles. Recently, it was reported
96 that differentiation states of mouse hindgut-derived cells were successfully maintained
97 for a relatively long period of time in a serum-free culture medium (Wang et al., 2018).
98 In that study, many types of gut-derived cells including not only ENS, ICC, SMCs but
99 also glial cells and serosa were observed, and this large and complex cell mass was seen
100 to undergo rhythmic contractions *in vitro*.
101 It has widely been appreciated that organoids can serve as a powerful models
102 and tools to circumvent such obstacles of organ complexity. Their relatively simple
103 structures allow analyses at higher resolution than *in vivo*, and also permit analyses of cell
104 behaviors in three-dimensional (3D) environment, which might be different from
105 behaviors *in vitro* behaviors confined to two dimensions. In the current study, we have
106 developed a novel organoid called "gut contractile organoid" by culturing chicken
107 hindgut-derived cells in a serum-free medium. The gut contractile organoid undergoes
108 periodic contractions, and it is essentially composed of ICCs and SMCs, the former
109 residing centrally whereas the latter peripherally, allowing distinction between the two
110 cell types in living organoids. These advantages enabled GCaMP-live imaging of Ca^{2+}
111 dynamics and revealed coordinated oscillations of Ca^{2+} transients between ICC-ICC,
112 SMC-SMC and SMC-ICC. Pharmacological studies further suggested that gap junctions
113 play a role in an ICC-to-SMC signaling, and also a possible feedback from SMC's
114 contractions to ICC's pace-making activities. In addition, by regarding a single organoid
115 as an oscillator unit and by placing oscillators separately in a hydrogel mold, we found
116 that two oscillators with different rhythm become synchronized when mediated by SMCs,
117 supporting the notion of SMC' contribution to ICC's pace-making. The gut contractile
118 organoid developed in this study must be useful to unveil the intrinsic mechanisms
119 underlying the rhythm coordination between/among ICCs and SMCs during peristaltic
120 movements in the embryonic gut.

121
122
123 **Results**

124 **Spheroids were formed from muscle layer-derived cells of the embryonic hindgut**

125 To develop a culture condition that would facilitate analyses of gut motility, we
126 dissected the muscle layer (also called *tunica muscularis*) from the hindgut of E15
127 embryos by removing the serosa and intestinal epithelium (mucosa) (Fig. S1). The
128 isolated muscle layer was dissociated into single cells to prepare 5.0×10^5 cells per culture
129 dish. We started analyses with a culture condition with FBS-free medium and Matrigel
130 as substrate as previously described for cultures in mice of gastrointestinal cells including
131 serosa (Wang et al., 2018). We tested three kinds of FBS-free media: DMEM/Ham's F-
132 12, Ham's F-12, and Neurobasal media (see Materials and Methods). When cultured in
133 DMEM/Ham's F-12 or Ham's F-12, dissociated cells formed very small aggregates
134 containing several cells at day 1, the morphology of which did not change significantly
135 until day 5 (Fig. 1A). In clear contrast, when cultured in the Neurobasal medium, cells
136 formed clusters that were interconnected by elongated cells with neighboring clusters as
137 early as day 1. These clusters grew as larger aggregates by day 3, and became spherical
138 by day 5. Such spheroids were not observed in the conditions with Ham's F-12 or
139 DMEM/Ham's F-12. We also tested different substrates, Poly-Lysine or collagen for dish
140 coating with the Neurobasal medium, but neither one yielded spheroid. To know how the
141 spherical aggregates were formed under the condition of Neurobasal medium and
142 Matrigel, we took time-lapse images at two-hour intervals. Originally sparse clusters that
143 were loosely connected by extended cells merged each other forming progressively larger
144 clusters (Fig. 1B, Movie 1). In the following experiments, we focused on the spheroids
145 formed under the condition of Neurobasal medium and Matrigel coating.
146

147 **The gut muscle layer-derived spheroids displayed periodic contractions**

148 The spheroids underwent reiterative contractions at day 3, and these contractions
149 were observed at least until day 7 of culture (Fig. 2A, Movie 2). Time-lapse imaging of
150 the contractions combined with quantitative assessments by ImageJ (see Materials and
151 Methods) showed that the average frequencies of contractions in each cluster/spheroid
152 at day 3, day 5, and day 7, were 3.32, 3.04, and 2.97 contractions/min, respectively (Fig.
153 2B), which largely corresponded to the rhythm of the E16 chicken embryonic intact gut
154 (Chevalier et al., 2019).
155

156 **The contracting spheroid was composed of ICCs and SMCs**

157 To determine the cell types comprising the spheroids, we performed
158 immunostaining with antibodies for the chicken c-Kit protein (for ICCs; Yagasaki et al.,
159 2022) and αSMA (for SMCs). It is known that ICCs and SMCs are derived from common
160 progenitors which are c-Kit^{+}/αSMA^{+}, and that after differentiation ICCs and SMCs are c-
161 Kit^{+}/αSMA^{-} and c-Kit^{-} /αSMA^{+}, respectively (Duband et al., 1993; Kluppel et al., 1998).
162 In the clusters at day 3, c-Kit^{+}/αSMA^{-} signals were detected in the internal region, and c-
163 Kit^{+}/αSMA^{+} signals at the periphery (Fig. 3A, Day 3), suggesting that internal cells were
164 differentiated ICCs, whereas peripheral cells were ICC/SMC progenitors. At day 5
165 onward, c-Kit^{+}/αSMA^{-} cells and c-Kit^{-}/αSMA^{+} cells were segregated which were located
166 internally and peripherally, respectively (Fig. 3A, Day 5), and this spatial segregation of
167 the cells remained unchanged until day 7 (Fig. 3A, Day 7), the latest stage examined in
168 this study. Infection of RCAS-GapEGFP into a forming spheroid further visualized
169 multipolar ICCs in the internal region (Fig. 3B), known to be characteristic of ICC-MY
170 which would normally reside in the layer of myenteric plexus (Mei et al., 2009; Sanders
171 et al., 2014). ICCs of a different type were also recognized, which were elongated, thin,
172 and lining underneath the peripheral SMCs (Fig. 3A, Day 7). It is possible that they were
173 ICC-IM, known to be embedded in and tightly associated with smooth muscles in the gut
174 (Huizinga et al., 2011; Iino & Horiguchi, 2006). Unexpectedly, the spheroid contained
175 few neural cells (ENS), if any, revealed by anti-Tuj1 antibody (Fig. S2).
176 Since ICCs and SMCs were spatially segregated in the sphenoid, we stained with
177 anti N-cadherin antibody (E-cadherin is positive solely in the mucosa/endoderm)
178 (Graham et al., 2017; Grosse et al., 2011). N-cadherin signals were seen in the internal
179 ICCs, and not in the peripheral SMCs (Fig. 3C). Thus, it is likely that N-cadherin plays a
180 role in the segregation.
181 In summary, the hindgut-derived spheroid displays three prominent
182 characteristics: (1) a dominant occupation by ICCs and SMCs with neglectable
183 contribution by ENS, (2) self-organization ability of internal ICCs encapsuled by a thin
184 layer of SMCs, (3) contractions with periodic rhythm. Based on these characteristics, we
185 designated this spheroid as "gut contractile organoid".
186
187 **Contraction-associated intracellular Ca^{2+} transients were coordinated between**
188 **ICCs and SMCs in the gut contractile organoid**
189 It has been reported that Ca^{2+} dynamics are important for pacemaker activity in
190 ICCs and contractions of SMCs. Ca^{2+} flows into ICCs via voltage-dependent Ca^{2+}
191 channels and propagates to SMCs, causing the gut muscle contractions (Baker et al.,
192 2021). We therefore investigated the Ca^{2+} dynamics in our gut contractile organoids.

193 Organoid-forming cells were infected with a RCAS-vector encoding GCaMP6s, a Ca^{2+}
194 indicator that emits EGFP fluorescence in response to Ca^{2+} influx, and mRuby3 as a
195 reporter (Fig. 4A). GCaMP6s-organoids were subjected to time-lapse imaging analyses
196 by confocal microscopy. As expected, the oscillations rhythm of Ca^{2+} transients as a
197 whole organoid was concomitant with that of contractions (Fig. 4B, Movie 4).
198 Taking advantage of the spatial segregation between ICCs (internal) and SMCs
199 (peripheral) (Fig. 3A), we compared the Ca^{2+} oscillation rhythm among ICCs and SMCs
200 (homotypically) and between ICC-SMC (heterotypically). We set up 3 regions of interests
201 (ROIs) in the central region, with one ROI corresponding to one cell, and captured the
202 Ca^{2+} transients. The three ROIs exhibited a synchronous pattern of Ca^{2+} oscillations (Fig.
203 4C, ICCs). Similarly, Ca^{2+} oscillations in three ROIs in the SMC layer were synchronous
204 (Fig. 4C, SMCs). These data highlight active communications taking place intercellularly
205 within ICCs and SMCs, respectively. We further compared Ca^{2+} oscillations between
206 ICC-SMC. Setting up with one ROI in an ICC, and one in a SMC. Again, the Ca^{2+} rhythm
207 was synchronized between these heterotypic cell types (Fig. 4C, ICC/SMC). With a closer
208 look, a rise of the Ca^{2+} transient in the ICC preceded that in SMC with a time lag (also
209 called latency) of 690 msec in average (Fig. 4C, ICC/SMC), suggestive of a propagation
210 of Ca^{2+} signals from ICC to SMC consistent with previous reports (Baker et al., 2021).
211
212 **Gap junction plays a role in ICC-to-SMC signaling**
213 Although a series of gut motility studies have proposed an importance of gap
214 junctions, rigid evidence has been limited due to a lack of experimental model. Our gut
215 contractile organoid should prove useful for clarifying the roles of gap junctions in the
216 synchronous motility, since intercellular synchronization was observed between/among
217 identifiable cells (ICCs and SMCs) as shown above. We performed pharmacological
218 assessments using gap junction inhibitors including carbenoxolone (CBX) and 18β-
219 glycyrrhetinic acid (18β-GA; Chevalier, 2018; Takeda et al., 2005), two of the most
220 widely used pharmacological inhibitors used to study gap junctions.
221 Following inhibitor administration into day 7 culture medium, organoids were
222 allowed to rest for 30 min to exclude possible effects by the administration, for example,
223 turbulence of the medium. With CBX or 18β-GA in the culture medium, the periodic
224 contraction of an organoid was retained with almost the same frequency as the control
225 (Fig. S3, Movie 3). We then examined whether the intercellular
226 synchronization/coordination was affected by the inhibitors. Similarly to Fig. 4, three
227 ROIs were set either in ICCs or SMCs territories for assessment of Ca^{2+} transients. The
228 same cells in a single organoid were tracked for their Ca^{2+} transients before and after the

229 inhibitor administration. Contrary to our expectation, none of 10 μM, 20 μM and 100 μM
230 concentrations of these inhibitors showed detectable inhibition of the synchronous
231 patterns of Ca^{2+} transients (Fig. 5A, B show 100 μM of CBX, Movie 5).
232 In contrast, when an ICC and SMC were compared, the preceding rise of Ca^{2+}
233 transient in ICC was abolished, although overall synchronization was retained between
234 these the cells (Fig. 5C). Collectively, while the contribution by gap junction to the
235 periodic contraction and intercellular synchronization in the organoid is relatively limited,
236 the ICC-to-SMC signals require gap junction-mediated communications, at least partly.
237
238 **Blebbistatin abolished organoidal contractions and oscillatory patterns of Ca^{2+}**
239 **transients**
240 Toward searching for factors that regulate the coordination between/among ICCs
241 and SMCs, we tested blebbistatin, a specific inhibitor of myosin II, which was expected
242 to cease organoidal contractions. Experimental procedures were similar to those for gap
243 junction inhibitors. We found that blebbistatin ceased periodic contractions of organoids
244 in a concentration-dependent manner, with 10 μM ceasing it completely (Fig. 6A, Movie
245 6). We examined Ca^{2+} transients in these contraction-inhibited organoids. Markedly,
246 periodic Ca^{2+} transients not only in SMCs, but also in ICCs were extinguished, resulting
247 in no/little synchronous Ca^{2+} patterns among and between ICCs and SMCs (Fig. 6B-E).
248 Although the possibility is not excluded that blebbistain directly inhibited non-muscle
249 myosin II in ICCs, these findings imply that the contractility feeds back to ICCs to
250 generate their periodic rhythm.
251
252 **Inter-organoidal coordination was mediated by SMCs**
253 During analyses with our novel organoids, we found that they easily fuse to each
254 other, suggesting that organoids grow by progressive fusion (Fig. 7A, Movie 7). This also
255 raised the possibility that the synchronous Ca^{2+} transients among organoid-constituting
256 cells (Fig. 4C) might be a consequence of phasic coordination upon the fusion of multiple
257 organoids that had shown different oscillatory phases. To test this possibility, we
258 transferred two organoids in a petri dish, and allowed them to fuse. Before the fusion,
259 Ca^{2+} oscillatory rhythm was indeed out of phase in the two organoids (Fig. 7B, Movie 8).
260 Markedly, upon fusion by 24 hours, their rhythm became in phase/synchronous (Fig. 7B,
261 Movie 8).
262 Since we noticed that cellular protrusions were often observed around the time of
263 organoidal fusion, we reasoned that these cellular processes would mediate the fusion and
264 its subsequent synchronization of Ca^{2+} transients (Fig. 7C). To test this, we developed a

265 3-well hydrogel with narrow channels connecting the wells (Fig. 8A). Organoids were
266 placed separately in each well, which prevented the fusion of organoidal bodies, but
267 allowed extension of cellular processes through the narrow channels and contact with
268 each other (Fig. 8B). After 72 hours of placement of organoids, cellular processes as well
269 as several cell bodies were present within the channel, and Ca^{2+} transients became
270 synchronized among the three organoids (Fig. 8C, Movie 9). However, with careful
271 examination, we also noticed that organoid-derived cells crawled out from the wells to
272 cover the top surface of the hydrogel, connecting the three organoids (Fig. 8D). Thus,
273 another possibility was raised that these crawled out cells would mediate the inter-
274 organoidal synchronization.
275 To test this possibility, we prepared a 3-well hydrogel in which the three wells
276 were disconnected (no channels) so that organoid-derived cellular processes were not able
277 to connect each other (Fig. 8E). By 3 days of culture, the top surface of the hydrogel was
278 indeed covered by cells in a similar way to Fig. 8D. These cells were positive for αSMA
279 but negative for c-Kit (Fig. 8F), indicating that they were SMCs that were somehow
280 detached and crawled out from the peripheral layer of the organoids. Importantly,
281 coincided with the top-coverage by the SMCs, the three organoids in the disconnected
282 wells displayed synchronized Ca^{2+} transients, highlighting the role of SMCs in mediating
283 coordination between organoids (Fig. 8G, Movie 10). Gap junction inhibitor yielded
284 no/little effects on the Ca^{2+} transient coordination (Fig. 8H, Movie 11).
285
286
287 **Discussion**
288 We have developed a novel gut contractile organoid, which displays several
289 unique characteristics: 1) it undergoes periodic contractions, 2) differentiation states of
290 ICCs (c-Kit^{+}/αSMA^{-}) and SMCs (c-Kit^{-}/αSMA^{+}) are maintained at least until day 7 in
291 the organoid, 3) the organoid is composed essentially of two types of cells, ICCs and
292 SMCs, with few ENS cells, if any, 4) ICCs (internal) and SMCs (peripheral) can be
293 distinguished for their localization in a living organoid, allowing 5) GCaMP-visualization
294 of Ca^{2+} transients and assessments of cell interactions between and among ICCs and
295 SMCs. These characteristics circumvent, at least partly, obstacles that have hampered
296 analyses in the research of gut peristalsis, such as unstable differentiation state of ICCs
297 and SMCs in cultures, and difficulties in identifying these cells in living preparations. In
298 studies of gut movements, how ICCs generate/maintain their periodic rhythm and how
299 ICCs and SMCs interact with each other have been long-standing questions, and our

organoids offer powerful advantages to address these and to understand the cellular mechanisms underlying the gut contractions/peristaltic motility.

Contrasting with many cases in organoid studies that have aimed at a *maximum* recapitulation of the intact organ, our gut contractile organoid is composed of a (probably) *minimum* number of cell types that suffice the generation and/or maintenance of rhythmic contractions, allowing high-resolution analyses at the cellular level. For example, adding ENS components to our organoid would allow the clarification of the role of ENS in the gut contraction. While the majority of internal cells in the organoid are ICCs (c-Kit^{+}/αSMA^{-}), the possibility cannot be excluded that platelet-derived growth factor receptor-α positive (PDFGRα^{+}/c-Kit^{-}/αSMA^{-}) cells, another type of interstitial cells (fibroblast-like cell) known to mediate neural activity to SMCs in the mouse gut (Sanders et al., 2024; Sanders et al., 2016), are included in our organoid. Available antibody against the chicken PDFGRα protein is awaited.

Coordinated Ca^{2+} transients in ICC/SMC populations in the gut contractile organoid

Measurement and quantification analyses with ICCs and SMCs that are identifiable in the living organoid revealed exquisite coordination of Ca^{2+} transients/oscillation homotypically between ICC-ICC and SMC-SMC and heterotypically between SMC-ICC (Fig. 4C). Notably, a rise (upstroke) of Ca^{2+} transient in ICCs precedes that of SMCs with a time lag (also called latency) of 690 msec, suggesting a directed signaling from ICC to SMC. These observations are consistent with previous studies using ICC- and SMC-specific transgenic mice that expressed GCaMP and RCaMP, respectively (Baker et al., 2021). In that study, the authors assessed Ca^{2+} transients in submucosal ICCs (ICC-SM) and compared them with those in their adjacent circular muscles, and showed that the rise of GCaMP signal preceded that of RCaMP with a latency of 56 +/- 14 msec. With these observations, they concluded that ICC-SM signals to its adjacent SMCs. In our study, time-lapse imaging was mostly performed with 700 msec intervals. Further studies with shorter intervals are awaited to know the latency time would be shorter than 690 msec in average.

Contribution of gap junction to ICC-to-SMC signaling

Effects by the block of gap junction by CBX or 18β-GA were relatively limited in our organoid assays: synchronous patterns of Ca^{2+} transients remained unchanged between SMC-SMC and ICC-ICC. In contrast, signaling from ICCs to SMCs was specifically affected by these inhibitors, in which the preceding rise of Ca^{2+} transient in

336 ICCs was abolished. The contribution of gap junction to the ICC-to-SMC signaling was
337 previously reported in mouse gut, which was from intramuscular ICCs (ICC-IM) to their
338 adjacent circular smooth muscles. However, interpretation of the role of gap junction in
339 ICC-SMC interactions, in general, has been under big debate. Some studies reported that
340 CBX or 18β-GA failed to inhibit these interactions or peristaltic motilities (Komuro et al.,
341 1996; Rohr et al., 1998; Schultz et al., 2003), or that electron microscopy did not detect
342 structures of gap junction in longitudinal muscles (Cousins et al., 2003; Daniel & Wang,
343 1999; Gabella & Blundell, 1981). Contribution of gap junctions to the gut motility appears
344 to be highly variable in different regions of gastrointestinal tract, for example, stomach
345 versus colon (Iino et al., 2007; Yang et al., 2012) . And a detection of gap junction
346 structures or mRNA/protein of Connexins (Cx; a component of gap junction) does not
347 necessarily mean that the gap junction is functional. Dominant negative form of gap
348 junction might be useful. Currently, ICC- or SMC-specific gene manipulations in our
349 organoid are not available, and further studies are awaited. It is intriguing that the
350 coordination between SMC-SMC and ICC-ICC was unaffected by the inhibitors in our
351 organoids. The possibility cannot be excluded that gap junctions that are not inhibited by
352 CBX or 18β-GA might operate. However, since these two inhibitors have popularly been
353 used to block a wide range of gap junctions, alternative possibility arises that cell
354 communications particularly between SMC-SMC are mediated by other mechanisms than
355 gap junctions, including mechanical signals as recently shown for coordinated Ca^{2+}
356 signaling in cardiac muscle cells (Fukui et al., 2021).
357
358 **Possible feedback from SMC's contractility to ICC's oscillatory rhythm**
359 Blebbistatin prevented the contraction of the organoids, which was concomitant
360 with abrogation of Ca^{2+} transients in ICCs. Since it has been reported that thick myosin
361 fibers necessary for the contraction are found only in SMCs but not in ICCs
362 (Gherghiceanu & Popescu, 2005; Rumessen & Thuneberg, 1991, 1996; Sun et al., 2006),
363 it is likely that ICCs do not have contractile ability. Our observations therefore promote
364 the possibilities that ICC's pace-making activity requires its own non-muscle myosin II,
365 and/or mechanical feedback by contracting SMCs. Currently, techniques that distinguish
366 between these possibilities are unavailable. Nevertheless, if it is the latter case, it would
367 indicate a signaling from SMC to ICC, the direction of which is unprecedented, since
368 previous literatures had shown that it was solely an ICC-to-SMC signaling process that
369 dictated the rhythm of SMC's contraction. We presume that the SMC's contribution to
370 ICC's pace-making is highly possible since this notion is further supported by other

371 findings obtained in this study showing that SMCs mediate inter-organoidal phase
372 coordination (Fig. 8) as more discussed below.
373 It is of note that the reciprocal interactions between pace-making cells and their
374 effectors have been reported in studies of neural circuit establishment. Spontaneous
375 activities emerging in motor neurons during embryogenesis are regulated by feedback
376 from their governing muscle's contractions so that motor neurons get organized to display
377 coordinated and stable oscillatory activities (Zeng et al., 2021). Thus, it is tempting to
378 speculate that during early gut peristalsis, ICCs might receive feedback from their
379 governing SMCs to generate more stable coordination of pace-making activity among
380 ICCs. Indeed, we have previously reported that in the very early embryonic gut, origins
381 of peristaltic wave (OPW) are randomly distributed along the gut axis, but they later
382 become confined to specific sites showing that ICCs undergo more stable and coordinated
383 pace-making (Shikaya et al., 2022).
384
385 **Interactions between ICCs and SMCs in the gut contractile organoid**
386 The organoid developed in this study was derived from the muscle layer (also
387 called *tunica muscularis*) of chicken E15 hindgut devoid of mucosa and serosa, in which
388 myenteric ICCs (ICC-MY), intramuscular ICCs (ICC-IM), and submucosal ICCs (ICC-
389 SM) are localized in a way similar to those in mice, shown by staining with antibody
390 against the chicken c-Kit protein (Yagasaki et al., 2022). In the current study, c-Kit
391 antibody-staining showed two types of cells in morphology in the gut contractile
392 organoid: one is multipolar and N-cad-positive ICCs located centrally, and the other is
393 ICCs that are thin in shape, N-cad negative, and lining beneath the most external layer of
394 SMCs. Based on the knowledge obtained in studies with mammalian species that ICC-
395 MY are multipolar whereas ICC-IM are bipolar and tightly associated with adjacent
396 SMCs (Huizinga et al., 2011; Iino & Horiguchi, 2006), it is conceivable in our organoids
397 that the central cells are ICC-MY, and the peripherally lining ones are ICC-IM. In
398 addition, it has been reported in mice that signaling from ICC-IM to SMCs is gap
399 junction-dependent. Collectively, our observations that gap junction-dependent signal
400 found between ICCs (central ICC) and SMCs in the organoid (Fig. 5C) could be
401 interpreted as follows: ICC-MY (central) signals to ICC-IM (second-most peripheral),
402 which in turn signals to the external SMCs mediated partly by gap junction. Such
403 sequences of signaling (ICC-MY to ICC-IM to SMCs) has also been proposed in the
404 intact gut in mammals, although rigid evidence has not been known. Direct comparison
405 of Ca^{2+} transients between the ICC-IM-like cells and SMCs in our organoid was

technically very difficult since these two cells were both thin and tightly associated each other.

The gut contractile organoid provides a useful model and tool for studying phasic coordination of oscillatory rhythm

To understand the gut peristaltic movements, which reiterate at specific sites along the gut axis (Shikaya et al., 2022), deciphering the mechanisms underlying the coordination/synchronization of oscillators among multiple cells is critical. Exploiting the finding obtained in the current study that multiple organoids easily fuse each other in vitro, we have found that two organoids with different oscillatory rhythm eventually coordinate their phases upon the fusion (Fig. 7). This suggests the ability of ICCs to adjust their rhythm to their neighbors. During identification of the rhythm-adjustment mediators using the 3-well hydrogel, contrasting with our original expectation, SMCs that were crawled out from the organoids and covered the top surface of the hydrogel were able to mediate the rhythm coordination among organoids (Fig. 8). Whether cellular thin protrusions connected with each other in narrow channels mediate the coordination remains undetermined. Nevertheless, our findings have revealed a novel role of SMCs in mediating rhythm coordination, and as discussed above, this supports the notion of a SMC-to-ICC signaling. It is unlikely that gap junction plays a major role in such signaling since gap junction inhibitor yielded no detectable effects in the assays using the 3-well hydrogel.

In summary, the gut contractile organoid developed in this study serves as a powerful model to study the establishment and maintenance of oscillatory rhythm (pace-making) and their coordination in the multicellular systems.

Materials and Methods

Chicken embryos

Fertilized chicken eggs were obtained from the Yamagishi poultry farms (Wakayama, Japan) and Takeuchi Farm (Nara, Japan). Embryos were staged according to embryonic days. All animal experiments were conducted with the ethical approval of Kyoto University (#202110).

Culture preparation of hindgut-derived cells

A hindgut was dissected from E15 chicken embryos (Fig. S1A), and cut into small pieces. After treating with 25 U dispase (Fujifilm Wako, 383-02281) /phosphate

442 buffer saline (PBS: 0.14 M NaCl, 2.7 mM KCl, 10 mM Na_2HPO_4-$12H_2O$, 1.8 mM
443 KH_2PO_4) at 38.5 °C for 40 min, serosa and intestinal epithelium were removed using
444 forceps. The muscle layer was minced into smaller pieces and treated with 0.2 mg/ml
445 collagenase (Fujifilm Wako, 038-22361) and 0.25 % trypsin/PBS at 37.0 °C for 30 min.
446 The reaction was stopped with 1 % FBS/PBS followed by centrifugation at 800 rpm for
447 3 min. The pellet was resuspended and washed in PBS followed by centrifugation. The
448 pellet was resuspended in culture medium, and 5.0×10^5 cells were plated in a glass bottom
449 dish (Matsunami, D11130H) treated with Matrigel (Corning, 354248) prepared in
450 advance at 38.5 °C for 20 min before use. Poly-lysine and collagen-coated dishes were
451 purchased (Matsunami, D11131H, D11134H). D-MEM /Ham's F-12 (Wako, 048-29785),
452 Ham's F-12 (Wako, 087-08335) and Neurobasal medium (Gibco, 21103-049) with 1× B-
453 27 supplement (Gibco, 17504044) and 0.5 mM L-glutamine were tested. After seeding,
454 time-lapse images were obtained with CM20 (Evident) under 5% CO_2 and 38.5°C with
455 2-hour intervals.
456
457 **Assessment of contraction in the spheroid/cluster**
458 The time-lapse images were obtained by confocal microscopy (Nikon, A1R)
459 under 5 % CO_2 and 38.5 °C. The bright field images were converted to the sequence of
460 Tiff images. Using ImageJ (National Institutes of Health, USA), these sequences were
461 divided into foreground and background automatically (Auto Threshold, mode "default")
462 and graphed by Plot Z-axis profile.
463
464 **Immunocytochemistry**
465 An organoid was fixed in acetic acid/ethanol (1:5) for 10 min at room
466 temperature (RT), and washed in PBS for 10 min at RT. The specimens were
467 permeabilized in 0.1% Tween-20 in PBS for 10 min at RT, followed by washing in PBS
468 for 10 min at RT. After blocking with 1 % blocking reagent for 1 hour at RT, specimens
469 were incubated overnight at 4 ℃ with dilution of 1:300 anti-c-Kit (Yagasaki et al., 2022),
470 1:300 Tuj-1 (RSD, MAB1195), 1:400 anti-αSMA antibody (Sigma-Aldrich, A5228),
471 and/or 1:200 anti-N-cadherin antibodies (TAKARA, M110) in 1% blocking regent
472 (Roche, 1096176)/PBS. Following three times washing in PBS for 10 min each at RT,
473 specimens were incubated for 1.5 hr at RT with 1:500 anti-rabbit IgG(H+L)-Alexa 488-
474 conjugated antibody (Donkey; Invitrogen, A21206), anti-mouse IgG_{2a}-Alexa 568-
475 conjugated antibody (Goat; Invitrogen, A21134), anti-rat IgG (H+L)-Alexa 488-
476 conjugated antibody (Goat; Invitrogen, A11006) and 1:2000 DAPI. After washing three
477 times in PBS for 10 min at RT, fluorescent images were obtained using the Nikon A1R

478 confocal microscope.
479
480 **Plasmids**
481 pAAV-hSynapsin1-GCaMP6s-P2A-mRuby3 was purchased from Addgene
482 (112007). Full-length cDNA of GCaMP6s was PCR-amplified:
483 forward 5'- GCGTACCACTGTGGCATCGATGCCACCATGGGTTCTCA -3',
484 reverse 5'- GCCCGTACATCGCATCGATTTACTTGTACAGCTCGT -3'.
485 The retroviral vector RCAS-EGFP was digested with Cla Ⅰ to remove EGFP, into which
486 a DNA fragment was inserted by In-Fusion HD Cloning Kit (TAKARA) to produce
487 RCAS-GCaMP6s-P2A-mRuby3. RCAS-GapEGFP is as previously described (Murai et
488 al., 2015)
489
490 **Preparation of retroviral vector particles**
491 RCAS-GCaMP6s-P2A-mRuby3 was transfected into the chicken fibroblast line
492 cells DF1 using Lipofectamin 2000 (Invitrogen). Transfected cells were cultured in 10
493 cm culture dish until confluent. The supernatant of transfected DF1 was collected for viral
494 precipitation, from which retroviral particles were prepared using Retro-Concentin™
495 Virus Precipitation Solution (SBI, RV100A-1).
496
497 **Intracellular Ca^{2+} imaging in the gut contractile organoid**
498 At day 2 or day 3 of cell culture, 10 mg/ml polybrene solution (final
499 concentration 4 μg/ml, Nacalai, 12996-81) and 20 μl opti-mem with above mentioned
500 virus particles were added to the culture medium to transfect GCaMP6s into organoid-
501 forming cells. The medium was replaced with fresh medium at day 5 and Ca^{2+} imaging
502 was performed at day 7. Time-lapse images were obtained using the confocal microscope
503 (Nikon, A1R) with 700 or 450 msec intervals, and exported intensity of each region of
504 interest (ROI) into an excel file by time measurement (Nikon, NIS-Elements). From the
505 excel file, the graphs were plotted with the fluorescence intensity by setting the beginning
506 of the measurement to zero.
507
508 **Drug administration**
509 Carbenoxolone (CBX; nacalai tesque, 32775-51) /H_2O, 18beta-Glycyrrhetinic
510 acid (18β-GA; abcam, ab142579)/DMSO and (-)-Blebbistatin (FUJIFILM Wako, 021-
511 17041) were prepared. Time-lapse images were acquired for a single organoid before and
512 after the drug administration. Following the drug adding, organoids were allowed to rest
513 for 30 min to avoid possible effect of turbulence of the medium, and time-lapse images

514 were taken for 5 min.
515
516 **Three-well hydrogel fabrication**
517 The photoinitiator P2CK was synthesized as previously reported (Li et al., 2013).
518 The target product was verified using proton NMR and Bruker's TopSpin software.
519 Gelatin-Norbornene was synthesized based on previous report (Van Hoorick et al., 2018).
520 The final reaction mixture was transferred to a dialysis tube (5-6 kDa; Spectra Por, cat.
521 no. 132680T) for dialysis against pure water at 40°C for 3 days. After dialysis, the
522 solution's pH was carefully adjusted to 8.0.
523 A piece of 3-well hydrogel was fabricated on a glass bottom dish (Matsunami)
524 from 100 μL of a solution containing 20 wt % Gelatin-Norbornene, 2 mM of the
525 photoinitiator P2CK, and 20 mM of crosslinker (DTT) (TCI, #D1071) using a two-photon
526 microscope with controllable laser power in 3D space according to the voxel file input
527 (Olympus, in house customized). The voxel files specifying the 3D shape of the hydrogel
528 were designed with Fusion 360 software. (Autodisk).
529
530
531 **Acknowledgement**
532 We thank Dr. Scott Gilbert for careful reading of the manuscript and discussion.
533 We also thank National BioResource Project (Chicken-Quail, Nagoya University) for
534 their technical help. This work was supported by JSPS KAKENHI Grant Numbers;
535 23H04933, 20H03259, 20K20520, 20K21425 for Y. T., and 21K06198, 23H04702 for
536 M. I., and FY 2022 Kusunoki 125 of Kyoto University 125th Anniversary Fund for M. I.,
537 and Ginpu Funds (Kyoto University) and incu-be fund (Leave a Nest Co., Ltd.) for R. Y..
538 R. Y. is an ex-fellow of JSPS.
539
540
541 **References**
542 Baker, S. A., Leigh, W. A., Del Valle, G., De Yturriaga, I. F., Ward, S. M., Cobine, C. A., Drumm,
543 B. T., & Sanders, K. M. (2021). Ca(2+) signaling driving pacemaker activity in
544 submucosal interstitial cells of Cajal in the murine colon. *Elife*, *10*.
545 https://doi.org/10.7554/eLife.64099
546 Barajas-Lopez, C., Berezin, I., Daniel, E. E., & Huizinga, J. D. (1989). Pacemaker activity recorded
547 in interstitial cells of Cajal of the gastrointestinal tract. *Am J Physiol*, *257*(4 Pt 1), C830-
548 835. https://doi.org/10.1152/ajpcell.1989.257.4.C830
549 Camborova, P., Hubka, P., Sulkova, I., & Hulin, I. (2003). The pacemaker activity of interstitial

550 cells of Cajal and gastric electrical activity. *Physiol Res*, *52*(3), 275-284.
551 https://www.ncbi.nlm.nih.gov/pubmed/12790758
552 Chevalier, N. R. (2018). The first digestive movements in the embryo are mediated by
553 mechanosensitive smooth muscle calcium waves. *Philos Trans R Soc Lond B Biol Sci*,
554 *373*(1759). https://doi.org/10.1098/rstb.2017.0322
555 Chevalier, N. R., Ammouche, Y., Gomis, A., Teyssaire, C., de Santa Barbara, P., & Faure, S. (2020).
556 Shifting into high gear: how interstitial cells of Cajal change the motility pattern of the
557 developing intestine. *Am J Physiol Gastrointest Liver Physiol*, *319*(4), G519-g528.
558 https://doi.org/10.1152/ajpgi.00112.2020
559 Chevalier, N. R., Dacher, N., Jacques, C., Langlois, L., Guedj, C., & Faklaris, O. (2019).
560 Embryogenesis of the peristaltic reflex. *J Physiol*, *597*(10), 2785-2801.
561 https://doi.org/10.1113/jp277746
562 Cousins, H. M., Edwards, F. R., Hickey, H., Hill, C. E., & Hirst, G. D. (2003). Electrical coupling
563 between the myenteric interstitial cells of Cajal and adjacent muscle layers in the guinea-
564 pig gastric antrum. *J Physiol*, *550*(Pt 3), 829-844.
565 https://doi.org/10.1113/jphysiol.2003.042176
566 Daniel, E. E., & Wang, Y. F. (1999). Gap junctions in intestinal smooth muscle and interstitial
567 cells of Cajal. *Microsc Res Tech*, *47*(5), 309-320. https://doi.org/10.1002/(SICI)1097-
568 0029(19991201)47:5<309::AID-JEMT2>3.0.CO;2-K
569 Duband, J. L., Gimona, M., Scatena, M., Sartore, S., & Small, J. V. (1993). Calponin and SM 22
570 as differentiation markers of smooth muscle: spatiotemporal distribution during avian
571 embryonic development. *Differentiation*, *55*(1), 1-11. https://doi.org/10.1111/j.1432-
572 0436.1993.tb00027.x
573 Fukui, H., Chow, R. W., Xie, J., Foo, Y. Y., Yap, C. H., Minc, N., Mochizuki, N., & Vermot, J.
574 (2021). Bioelectric signaling and the control of cardiac cell identity in response to
575 mechanical forces. *Science*, *374*(6565), 351-354.
576 https://doi.org/10.1126/science.abc6229
577 Gabella, G., & Blundell, D. (1981). Gap junctions of the muscles of the small and large intestine.
578 *Cell Tissue Res*, *219*(3), 469-488. https://doi.org/10.1007/BF00209987
579 Gherghiceanu, M., & Popescu, L. M. (2005). Interstitial Cajal-like cells (ICLC) in human resting
580 mammary gland stroma. Transmission electron microscope (TEM) identification. *J Cell*
581 *Mol Med*, *9*(4), 893-910. https://doi.org/10.1111/j.1582-4934.2005.tb00387.x
582 Graham, H. K., Maina, I., Goldstein, A. M., & Nagy, N. (2017). Intestinal smooth muscle is
583 required for patterning the enteric nervous system. *J Anat*, *230*(4), 567-574.
584 https://doi.org/10.1111/joa.12583
585 Grosse, A. S., Pressprich, M. F., Curley, L. B., Hamilton, K. L., Margolis, B., Hildebrand, J. D., &

586 Gumucio, D. L. (2011). Cell dynamics in fetal intestinal epithelium: implications for
587 intestinal growth and morphogenesis. *Development*, *138*(20), 4423-4432.
588 https://doi.org/10.1242/dev.065789
589 Huizinga, J. D., Martz, S., Gil, V., Wang, X. Y., Jimenez, M., & Parsons, S. (2011). Two
590 independent networks of interstitial cells of cajal work cooperatively with the enteric
591 nervous system to create colonic motor patterns. *Front Neurosci*, *5*, 93.
592 https://doi.org/10.3389/fnins.2011.00093
593 Huizinga, J. D., Thuneberg, L., Kluppel, M., Malysz, J., Mikkelsen, H. B., & Bernstein, A. (1995).
594 W/kit gene required for interstitial cells of Cajal and for intestinal pacemaker activity.
595 *Nature*, *373*(6512), 347-349. https://doi.org/10.1038/373347a0
596 Iino, S., & Horiguchi, K. (2006). Interstitial cells of cajal are involved in neurotransmission in the
597 gastrointestinal tract. *Acta Histochem Cytochem*, *39*(6), 145-153.
598 https://doi.org/10.1267/ahc.06023
599 Iino, S., Horiguchi, S., Horiguchi, K., & Nojyo, Y. (2007). Interstitial cells of Cajal in the
600 gastrointestinal musculature of W mutant mice. *Arch Histol Cytol*, *70*(3), 163-173.
601 https://doi.org/10.1679/aohc.70.163
602 Kito, Y., Ward, S. M., & Sanders, K. M. (2005). Pacemaker potentials generated by interstitial cells
603 of Cajal in the murine intestine. *Am J Physiol Cell Physiol*, *288*(3), C710-720.
604 https://doi.org/10.1152/ajpcell.00361.2004
605 Kluppel, M., Huizinga, J. D., Malysz, J., & Bernstein, A. (1998). Developmental origin and Kit-
606 dependent development of the interstitial cells of cajal in the mammalian small intestine.
607 *Dev Dyn*, *211*(1), 60-71. https://doi.org/10.1002/(SICI)1097-
608 0177(199801)211:1<60::AID-AJA6>3.0.CO;2-5
609 Komuro, T., Tokui, K., & Zhou, D. S. (1996). Identification of the interstitial cells of Cajal. *Histol*
610 *Histopathol*, *11*(3), 769-786. https://www.ncbi.nlm.nih.gov/pubmed/8839765
611 Li, Z. Q., Torgersen, J., Ajami, A., Mühleder, S., Qin, X. H., Husinsky, W., Holnthoner, W.,
612 Ovsianikov, A., Stampfl, J., & Liska, R. (2013). Initiation efficiency and cytotoxicity of
613 novel water-soluble two-photon photoinitiators for direct 3D microfabrication of
614 hydrogels. *Rsc Advances*, *3*(36), 15939-15946. https://doi.org/10.1039/c3ra42918k
615 Liu, L. W., Thuneberg, L., & Huizinga, J. D. (1998). Development of pacemaker activity and
616 interstitial cells of Cajal in the neonatal mouse small intestine. *Dev Dyn*, *213*(3), 271-282.
617 https://doi.org/10.1002/(SICI)1097-0177(199811)213:3<271::AID-AJA4>3.0.CO;2-R
618 Mei, F., Han, J., Huang, Y., Jiang, Z. Y., Xiong, C. J., & Zhou, D. S. (2009). Plasticity of interstitial
619 cells of cajal: a study in the small intestine of adult Guinea pigs. *Anat Rec (Hoboken)*,
620 *292*(7), 985-993. https://doi.org/10.1002/ar.20928
621 Murai, H., Tadokoro, R., Sakai, K., & Takahashi, Y. (2015). In ovo gene manipulation of

622 melanocytes and their adjacent keratinocytes during skin pigmentation of chicken
623 embryos. *Dev Growth Differ*, *57*(3), 232-241. https://doi.org/10.1111/dgd.12201
624 Rohr, S., Kucera, J. P., & Kleber, A. G. (1998). Slow conduction in cardiac tissue, I: effects of a
625 reduction of excitability versus a reduction of electrical coupling on microconduction. *Circ*
626 *Res*, *83*(8), 781-794. https://doi.org/10.1161/01.res.83.8.781
627 Rumessen, J. J., & Thuneberg, L. (1991). Interstitial cells of Cajal in human small intestine.
628 Ultrastructural identification and organization between the main smooth muscle layers.
629 *Gastroenterology*, *100*(5 Pt 1), 1417-1431.
630 https://www.ncbi.nlm.nih.gov/pubmed/2013387
631 Rumessen, J. J., & Thuneberg, L. (1996). Pacemaker cells in the gastrointestinal tract: interstitial
632 cells of Cajal. *Scand J Gastroenterol Suppl*, *216*, 82-94.
633 https://doi.org/10.3109/00365529609094564
634 Sanders, K. M., Drumm, B. T., Cobine, C. A., & Baker, S. A. (2024). Ca(2+) dynamics in
635 interstitial cells: foundational mechanisms for the motor patterns in the gastrointestinal
636 tract. *Physiol Rev*, *104*(1), 329-398. https://doi.org/10.1152/physrev.00036.2022
637 Sanders, K. M., Kito, Y., Hwang, S. J., & Ward, S. M. (2016). Regulation of Gastrointestinal
638 Smooth Muscle Function by Interstitial Cells. *Physiology (Bethesda)*, *31*(5), 316-326.
639 https://doi.org/10.1152/physiol.00006.2016
640 Sanders, K. M., Publicover, N. G., & Ward, S. M. (1991). Involvement of interstitial cells of Cajal
641 in pacemaker activity of canine colon. *J Smooth Muscle Res*, *27*(1), 1-11.
642 https://doi.org/10.1540/jsmr.27.1
643 Sanders, K. M., Ward, S. M., & Koh, S. D. (2014). Interstitial cells: regulators of smooth muscle
644 function. *Physiol Rev*, *94*(3), 859-907. https://doi.org/10.1152/physrev.00037.2013
645 Schultz, T., Daniel, V., & Daniel, E. E. (2003). Does ICC pacing require functional gap junctions
646 between ICC and smooth muscle in mouse intestine? *Neurogastroenterol Motil*, *15*(2),
647 129-138. https://doi.org/10.1046/j.1365-2982.2003.00401.x
648 Shikaya, Y., Takase, Y., Tadokoro, R., Nakamura, R., Inaba, M., & Takahashi, Y. (2022).
649 Distribution Map of Peristaltic Waves in the Chicken Embryonic Gut Reveals Importance
650 of Enteric Nervous System and Inter-Region Cross Talks Along the Gut Axis. *Front Cell*
651 *Dev Biol*, *10*, 827079. https://doi.org/10.3389/fcell.2022.827079
652 Sun, X., Yu, B., Xu, L., Dong, W., & Luo, H. (2006). Interstitial cells of Cajal in the murine
653 gallbladder. *Scand J Gastroenterol*, *41*(10), 1218-1226.
654 https://doi.org/10.1080/00365520600708800
655 Takaki, M. (2003). Gut pacemaker cells: the interstitial cells of Cajal (ICC). *J Smooth Muscle Res*,
656 *39*(5), 137-161. https://doi.org/10.1540/jsmr.39.137
657 Takayama, I., Horiguchi, K., Daigo, Y., Mine, T., Fujino, M. A., & Ohno, S. (2002). The interstitial

658 cells of Cajal and a gastroenteric pacemaker system. *Arch Histol Cytol*, *65*(1), 1-26.
659 https://doi.org/10.1679/aohc.65.1
660 Takeda, Y., Ward, S. M., Sanders, K. M., & Koh, S. D. (2005). Effects of the gap junction blocker
661 glycyrrhetinic acid on gastrointestinal smooth muscle cells. *Am J Physiol Gastrointest*
662 *Liver Physiol*, *288*(4), G832-841. https://doi.org/10.1152/ajpgi.00389.2004
663 Thomsen, L., Robinson, T. L., Lee, J. C., Farraway, L. A., Hughes, M. J., Andrews, D. W., &
664 Huizinga, J. D. (1998). Interstitial cells of Cajal generate a rhythmic pacemaker current.
665 *Nat Med*, *4*(7), 848-851. https://doi.org/10.1038/nm0798-848
666 Torihashi, S., Fujimoto, T., Trost, C., & Nakayama, S. (2002). Calcium oscillation linked to
667 pacemaking of interstitial cells of Cajal: requirement of calcium influx and localization of
668 TRP4 in caveolae. *J Biol Chem*, *277*(21), 19191-19197.
669 https://doi.org/10.1074/jbc.M201728200
670 Torihashi, S., Nishi, K., Tokutomi, Y., Nishi, T., Ward, S., & Sanders, K. M. (1999). Blockade of
671 kit signaling induces transdifferentiation of interstitial cells of cajal to a smooth muscle
672 phenotype. *Gastroenterology*, *117*(1), 140-148. https://doi.org/10.1016/s0016-
673 5085(99)70560-3
674 Van Hoorick, J., Gruber, P., Markovic, M., Rollot, M., Graulus, G. J., Vagenende, M., Tromayer,
675 M., Van Erps, J., Thienpont, H., Martins, J. C., Baudis, S., Ovsianikov, A., Dubruel, P., &
676 Van Vlierberghe, S. (2018). Highly Reactive Thiol-Norbornene Photo-Click Hydrogels:
677 Toward Improved Processability. *Macromol Rapid Commun*, *39*(14), e1800181.
678 https://doi.org/10.1002/marc.201800181
679 Wang, Q., Wang, K., Solorzano-Vargas, R. S., Lin, P. Y., Walthers, C. M., Thomas, A. L., Martín,
680 M. G., & Dunn, J. C. Y. (2018). Bioengineered intestinal muscularis complexes with long-
681 term spontaneous and periodic contractions. *PLoS One*, *13*(5), e0195315.
682 https://doi.org/10.1371/journal.pone.0195315
683 Yagasaki, R., Shikaya, Y., Kawachi, T., Inaba, M., Takase, Y., & Takahashi, Y. (2022). Newly raised
684 anti-c-Kit antibody visualizes morphology of interstitial cells of Cajal in the developing
685 gut of chicken embryos. *Dev Growth Differ*, *64*(8), 446-454.
686 https://doi.org/10.1111/dgd.12808
687 Yang, P., Yu, Z., Gandahi, J. A., Bian, X., Wu, L., Liu, Y., Zhang, L., Zhang, Q., & Chen, Q. (2012).
688 The identification of c-Kit-positive cells in the intestine of chicken. *Poult Sci*, *91*(9), 2264-
689 2269. https://doi.org/10.3382/ps.2011-02076
690 Zeng, X., Komanome, Y., Kawasaki, T., Inada, K., Jonaitis, J., Pulver, S. R., Kazama, H., & Nose,
691 A. (2021). An electrically coupled pioneer circuit enables motor development via
692 proprioceptive feedback in Drosophila embryos. *Curr Biol*, *31*(23), 5327-5340 e5325.
693 https://doi.org/10.1016/j.cub.2021.10.005

694 **Figures**

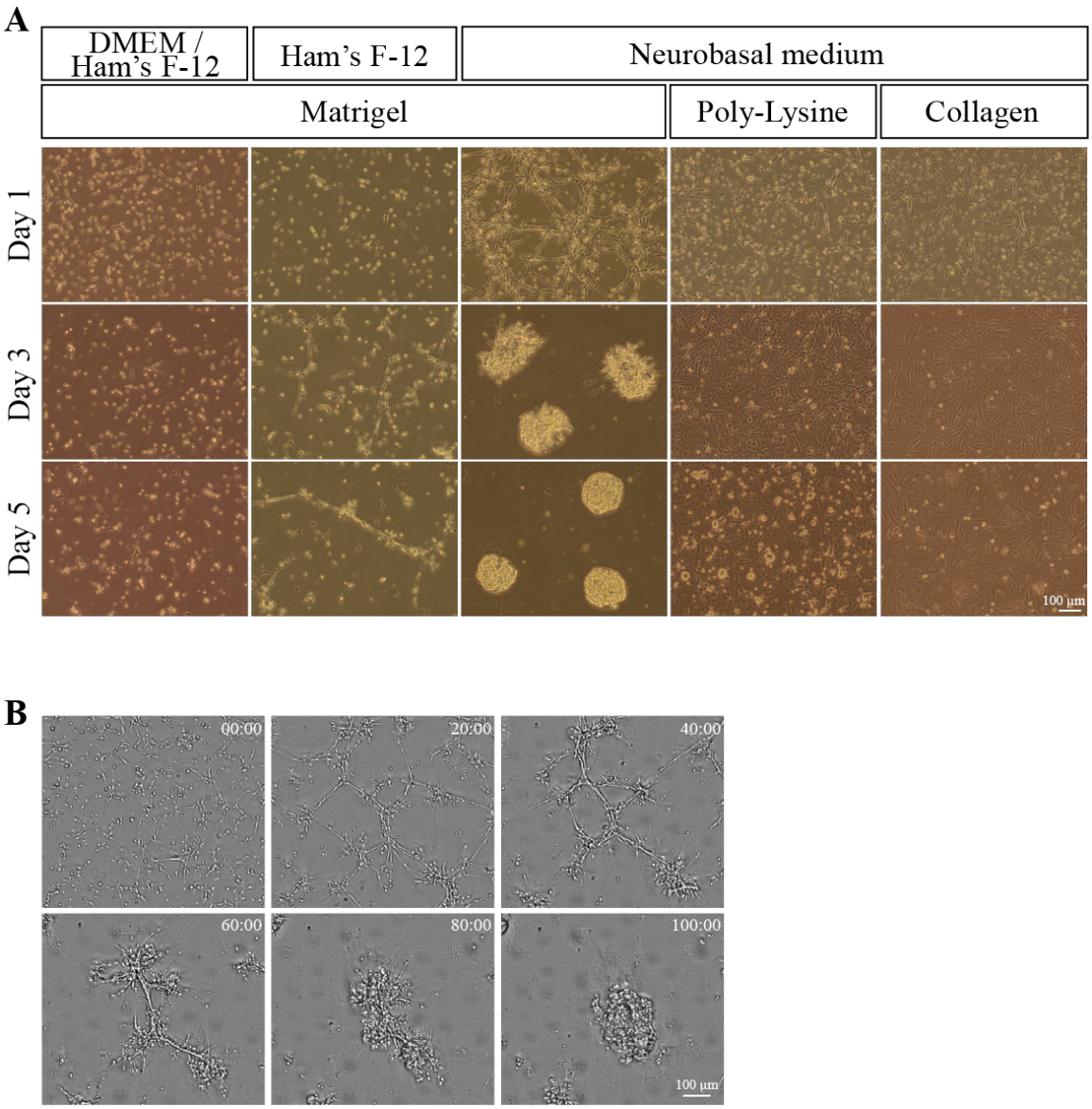

695

696 **Figure 1 Culture of muscle layer-derived cells prepared from embryonic hindgut.**
697 (A) Culture of muscle layer-derived cells prepared from embryonic hindgut with FBS
698 free-media and substrates. (B) Long-term time-lapse imaging after seeding on Matrigel
699 with Neurobasal media. The images show the ability of these cells to self-assemble at 0,
700 20, 40, 60, 80 and 100 hours taken from Movie 1. Scale bars: 100 µm in A, B.

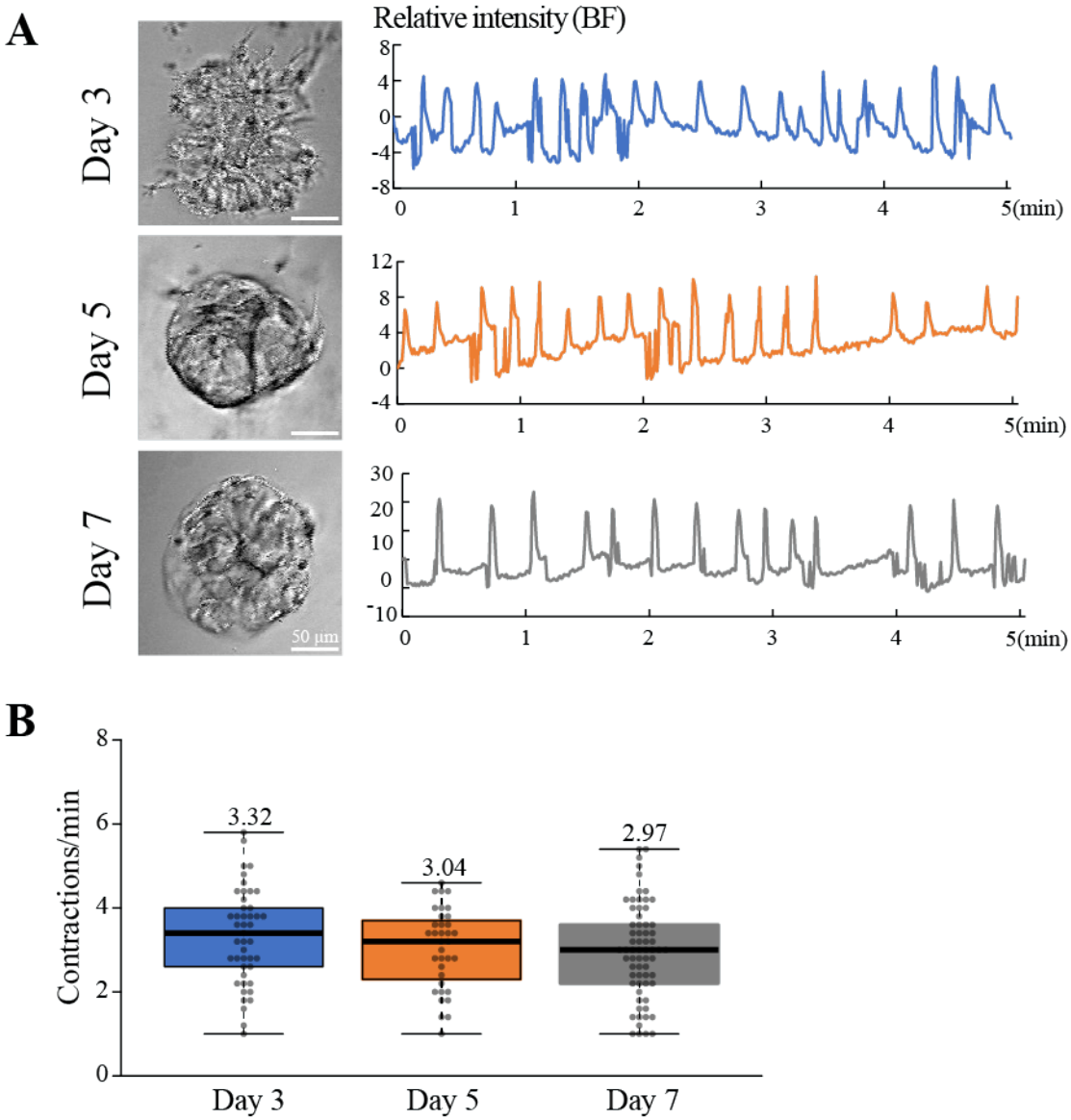

Figure 2 Forming spheroids exhibited reiterated contractions.
(A) Clusters/spheroids on day 3, 5 and 7 exhibited periodic contractions. Graphs show contractions quantified by differences in the intensity of brightfield in sequential images. (B) Frequency of contractions of the cluster/spheroid on day 3-7 (N=day 3: 46, day 5: 35, day 7: 60). The number on each graph shows the average of contraction frequencies. Scale bars: 50 µm in A.

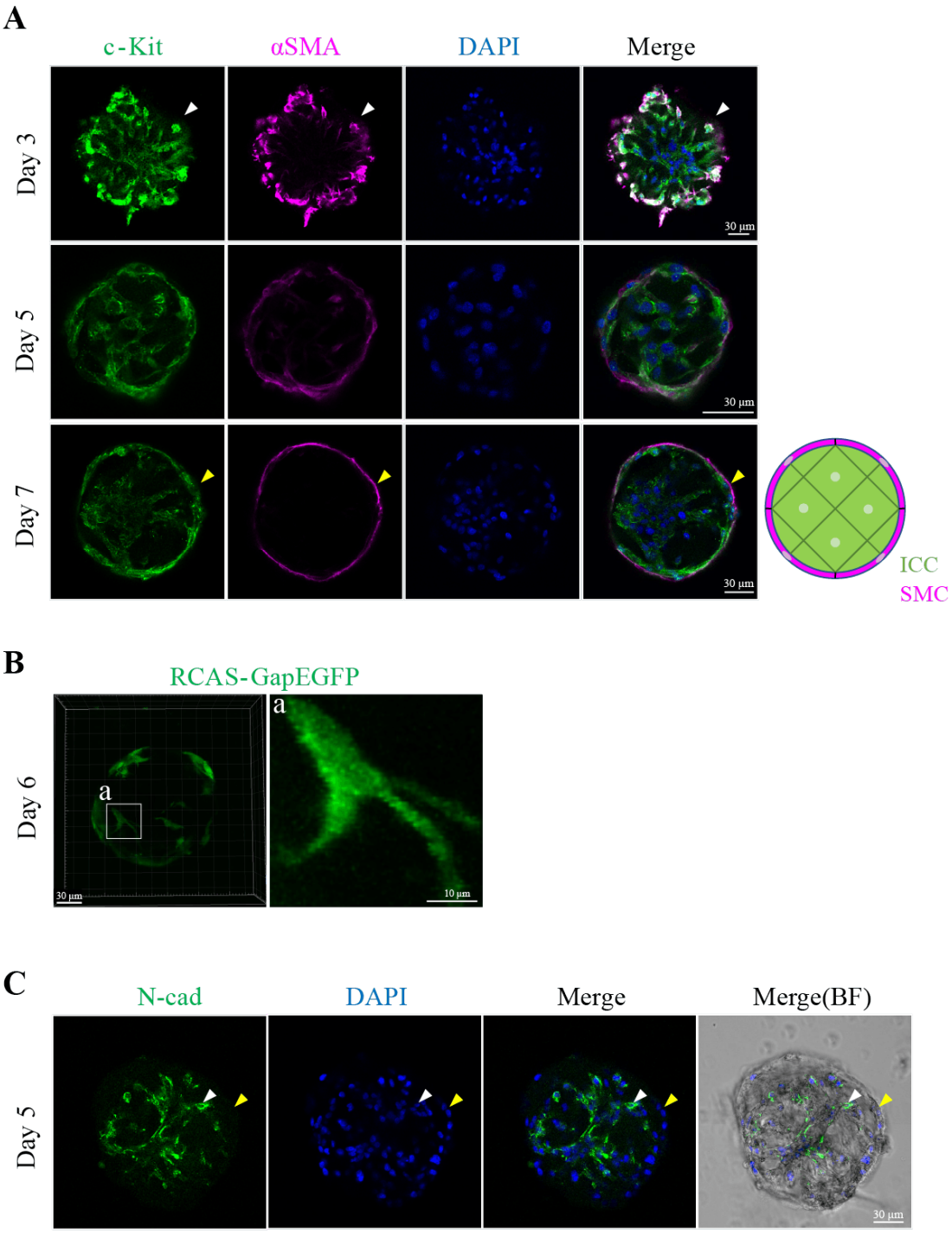

Figure 3 The cluster/spheroid is composed of ICCs internally and SMCs peripherally. (A) Co-staining with anti-c-Kit- and αSMA antibodies. White arrowheads show co-expression of c-Kit and αSMA at Day 3. Yellow arrowheads indicate a cell expressing αSMA but not c-Kit at day 7. A diagram shows an image of cell arrangement

713 (green: ICC, magenta: SMC) in the spheroid at day 7. (B) Cell morphology in the spheroid
714 at day 6 revealed by RCAS-gapEGFP expression. (C) Staining of spheroids at day 5 with
715 anti-N-cadherin antibody. A white arrowhead shows expression of N-cadherin. A yellow
716 arrowhead shows a cell which does not express N-cadherin in the outer region of the
717 spheroid. Scale bars: 30 μm in A-C, 10 μm in a.
718

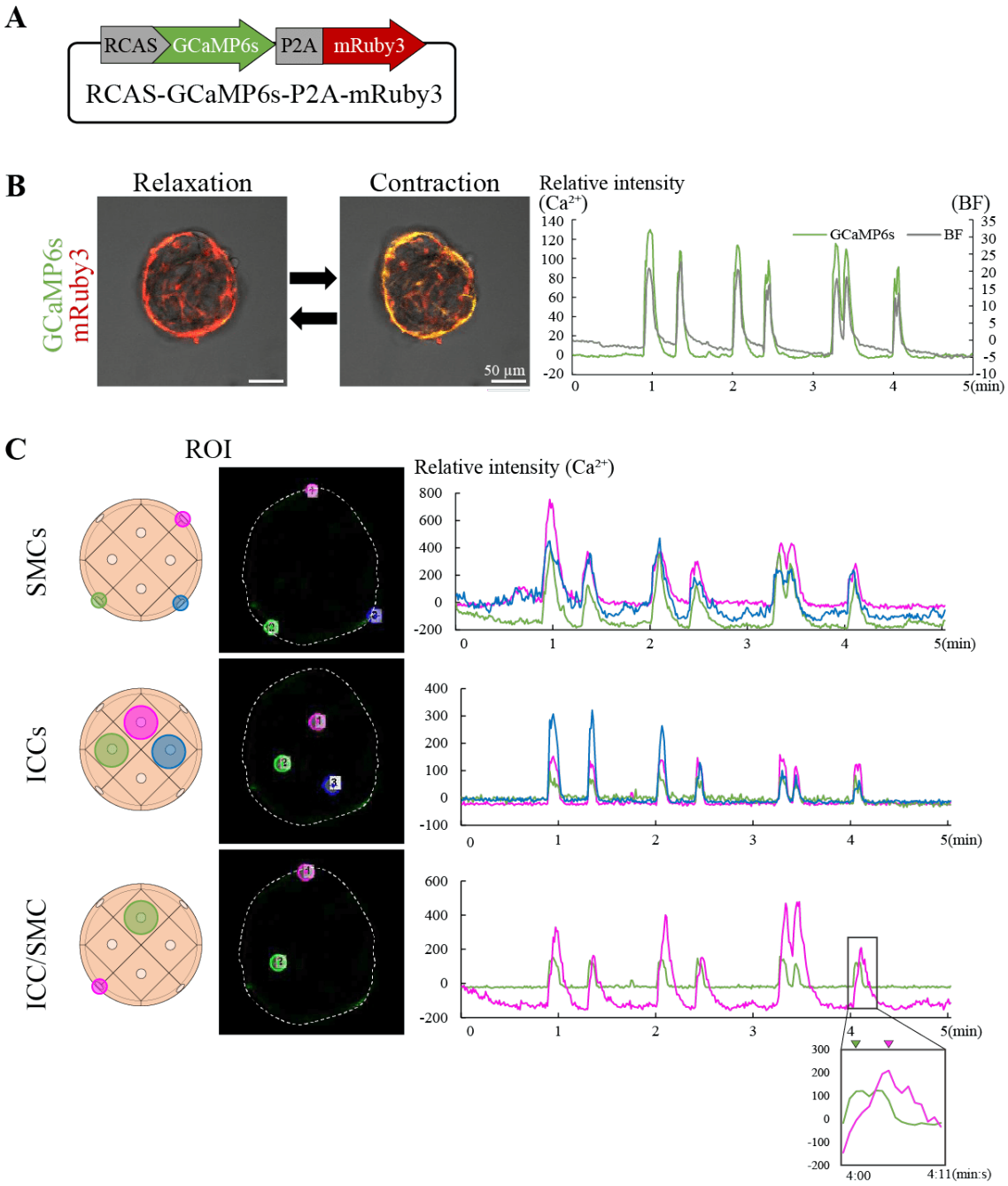

Figure 4 Ca^{2+} imaging of the gut contractile organoid revealed intercellular synchronization.

(A) RCAS-GCaMP6s-P2A-mRuby3 plasmid. (B) Ca^{2+} imaging of gut contractile organoid during relaxation and contraction. Ca^{2+} dynamics (green) and contraction (grey) of gut contractile organoid. (C) Simultaneous measurement of intercellular Ca^{2+} dynamics between ICC-ICC, SMC-SMC or ICC-SMC. Three or two ROIs with Ca^{2+} signal-positive cells were set in a single organoid. Graphs show Ca^{2+} dynamics in the

727 ROIs. Magnified view shows that a rise of Ca^{2+} signal in ICC (green) preceded that in
728 SMC (magenta). Scale bar: 50 μm in B.
729

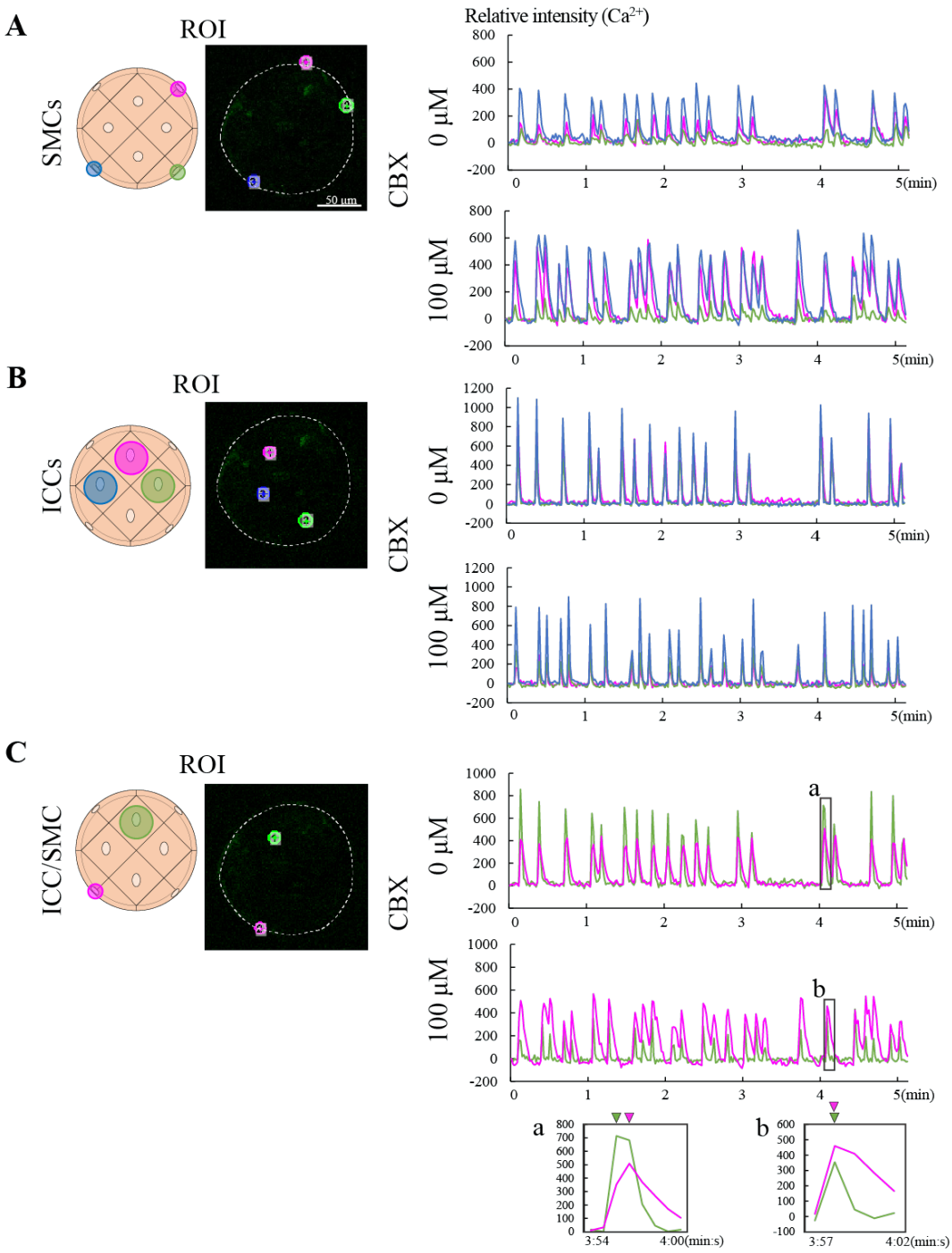

Figure 5 Gap junction inhibitor exerted limited effects on the synchronization of Ca^{2+} dynamics.

GCaMP6s-expressing organoids were cultured with CBX, and three or two ROIs were assessed for their Ca^{2+} synchronization. A single organoid was subjected to the assessment before (0 μM; control) and after administrations of 100 μM CBX. The

synchronization was unaffected between (A) SMC-SMC and (B) ICC-ICC, but that in (C) ICC-SMC was partially affected. Magnified view shows that the preceding rise of Ca^{2+} in ICC (green) before CBX was abrogated after CBX. Scale bar: 50 μm in A.

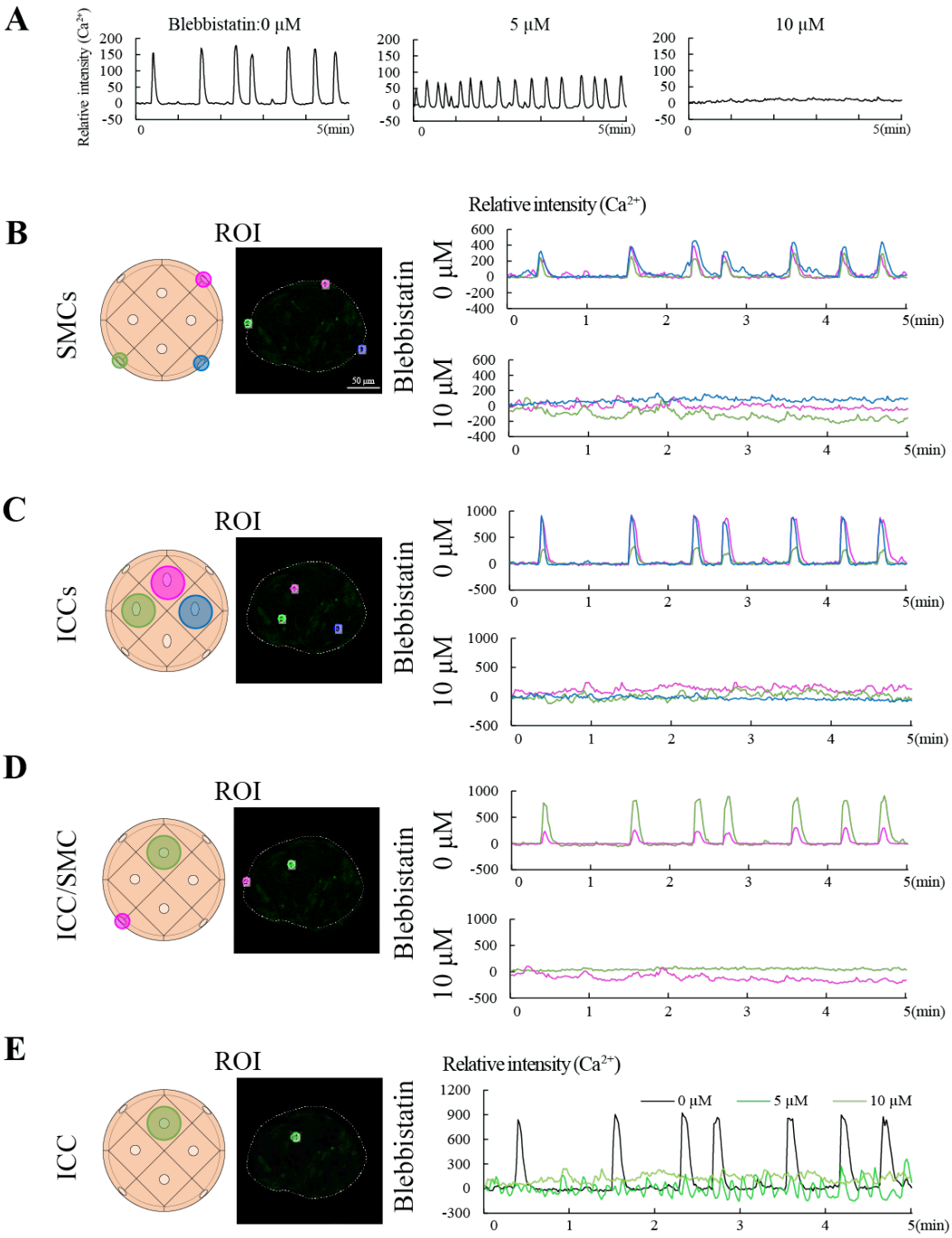

Figure 6 The organoidal contraction is important for Ca^{2+} dynamics in ICCs. GCaMP6s-expressing organoids were cultured with Blebbistatin. (A) Ca^{2+} oscillation was extinguished in the entire organoid by administration of Blebbistatin. (B-D) Ca^{2+} dynamics in (B) SMC-SMC, (C) ICC-ICC and (D) ICC-SMC. Three or two ROIs were assessed for their Ca^{2+} synchronization. A single organoid was subjected to the

746 assessment before (0 μM; control) and after administrations of 10 μM Blebbistatin. (E)
747 Ca^{2+} transients in a single ICC in 0 μM, 5 μM, and 10 μM. Scale bar: 50 μm in B.
748

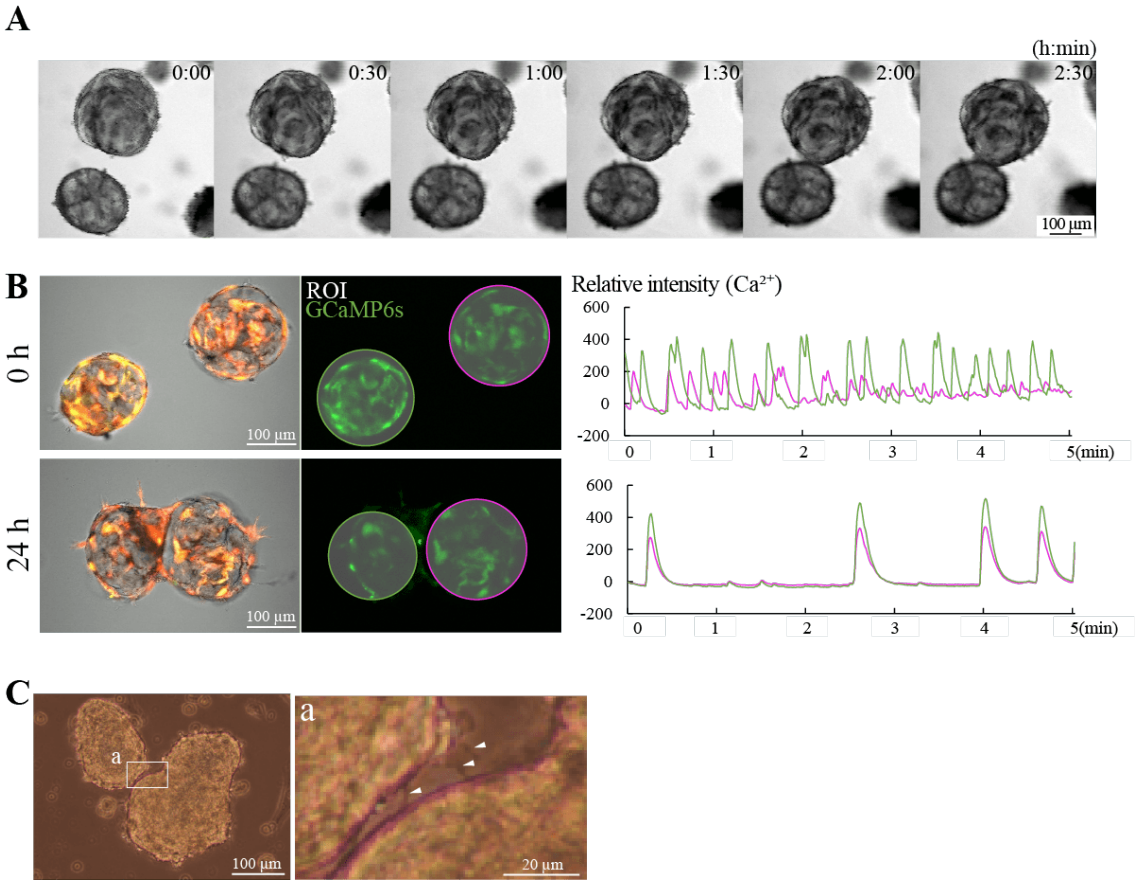

Figure 7 Ca^{2+} dynamics in multiple gut contractile organoids undergo synchronization upon their fusion.

(A) Time-lapse imaging of organoidal fusion. (B) When two organoids that originally showed independent rhythm of Ca^{2+} fused to each other, their rhythm became synchronized after fusion (24 h). (C) Protrusions between two neighboring organoids. White arrowheads show three protrusions from the left organoid. Scale bars: 100 µm in A-C, 20 µm in a.

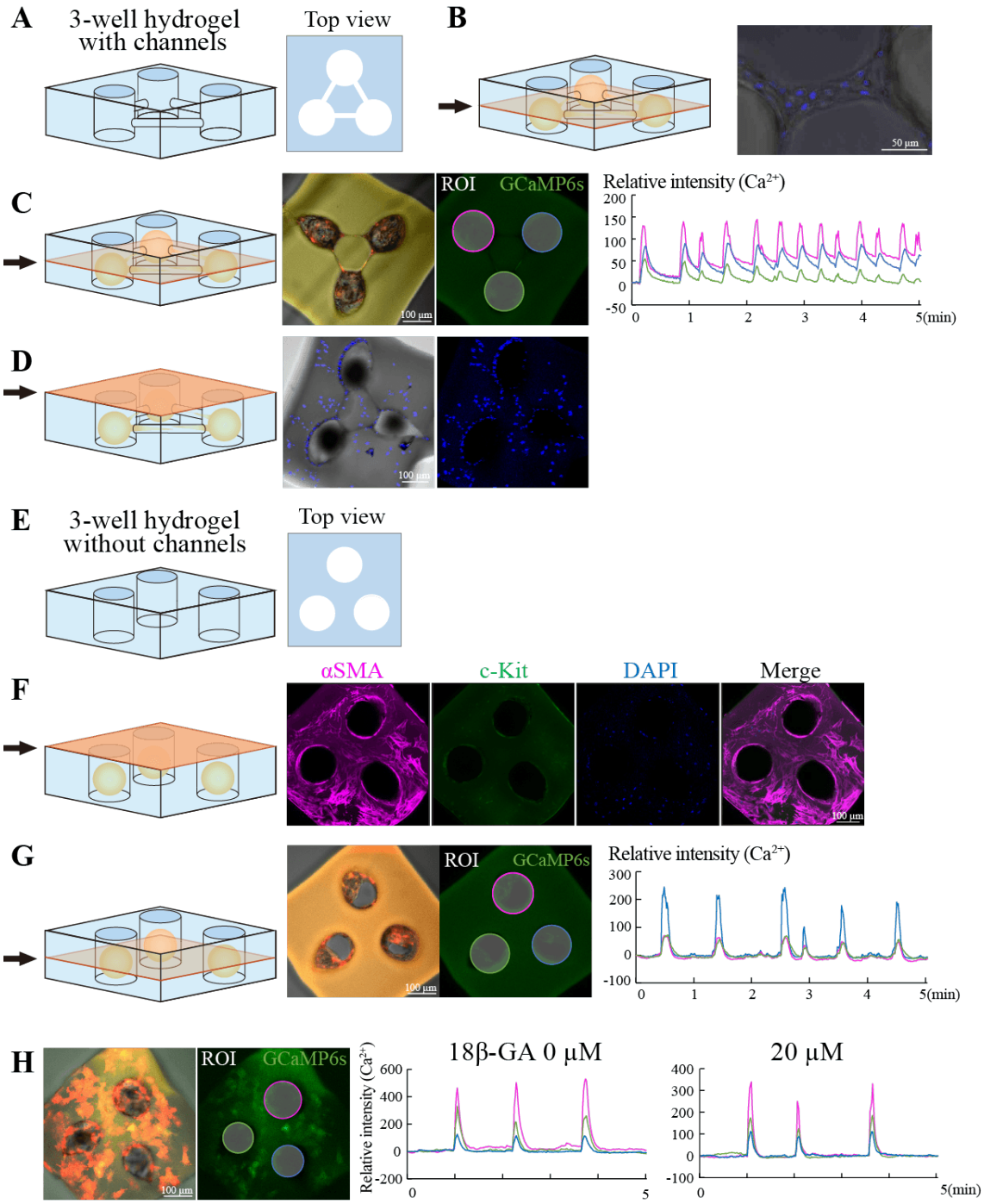

Figure 8 Smooth muscle cells mediate the Ca^{2+} synchronization between organoids. (A) Diagram of 3-well hydrogel in which an organoid placed in each well. This gel mold does not allow organoidal bodies to fuse to each other, but allow them to extend/migrate protrusions/cells through a narrow channel connecting the wells (B). (C) After 3 days, three organoids displayed synchronization of Ca^{2+} dynamics. (D) Some organoid-derived cells crawled out from the wells and covered the top surface of the hydrogel, resulting in

765 bridging the three unfused organoids. (E) Diagram of 3-well hydrogel *without* channels
766 (F) Surface-covering cells were SMCs (αSMA positive and c-Kit-negative). (G) In the
767 hydrogel without channels but with surface-covered SMCs, Ca^{2+} dynamics in the 3
768 organoids were synchronized. (H) The Ca^{2+} synchronization shown in (G) was not altered
769 by 18β-GA. Scale bars: 50 μm in B, 100 μm in C-H.
770
771

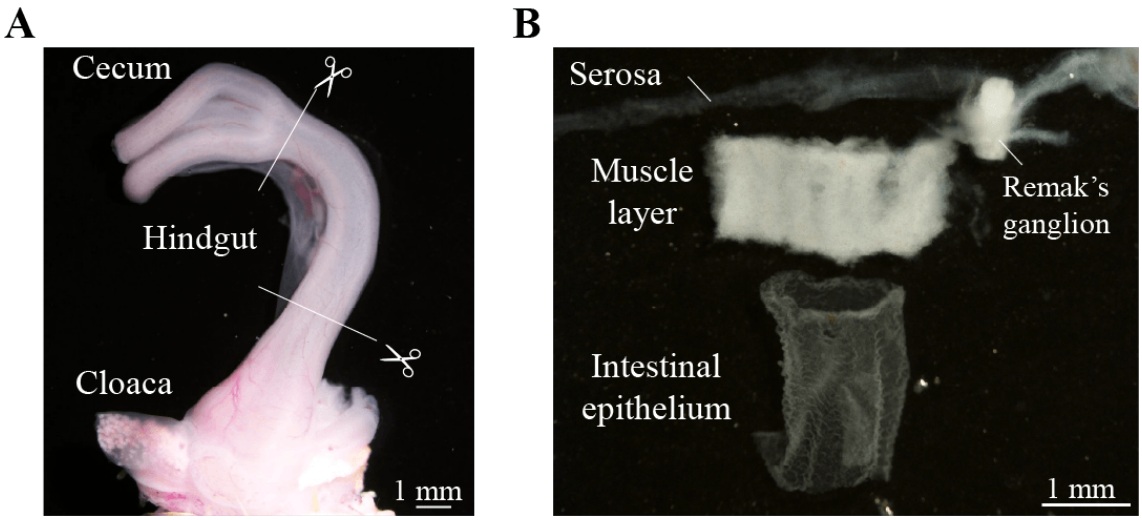

Supplementary Figure S1

(A) Chicken embryonic hindgut at E15. The hindgut was dissected from the bottom of the cecum to the front of the cloaca (white lines). (B) Three layers of E15 hindgut: serosa, muscle layer, intestinal epithelium. Remak's ganglion was also removed. Scale bars: 1 mm in A, B

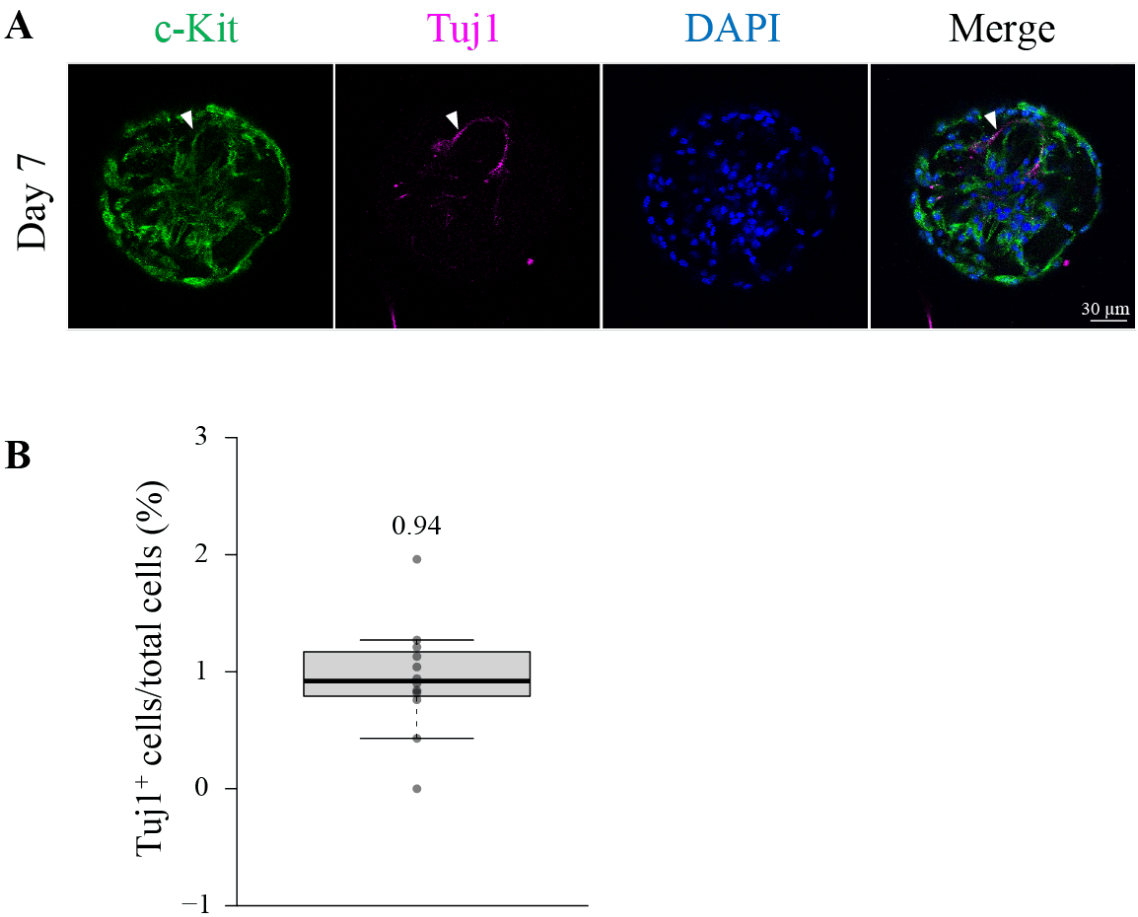

Supplementary Figure S2

(A) Co-staining of Day 7 organoids with anti-c-Kit- and Tuj1 antibodies. White arrowhead shows a Tuj1^{+} cell. (B) Representation of Tuj1^{+} cells in an organoid at day 7. Scale bar: 30 µm in A.

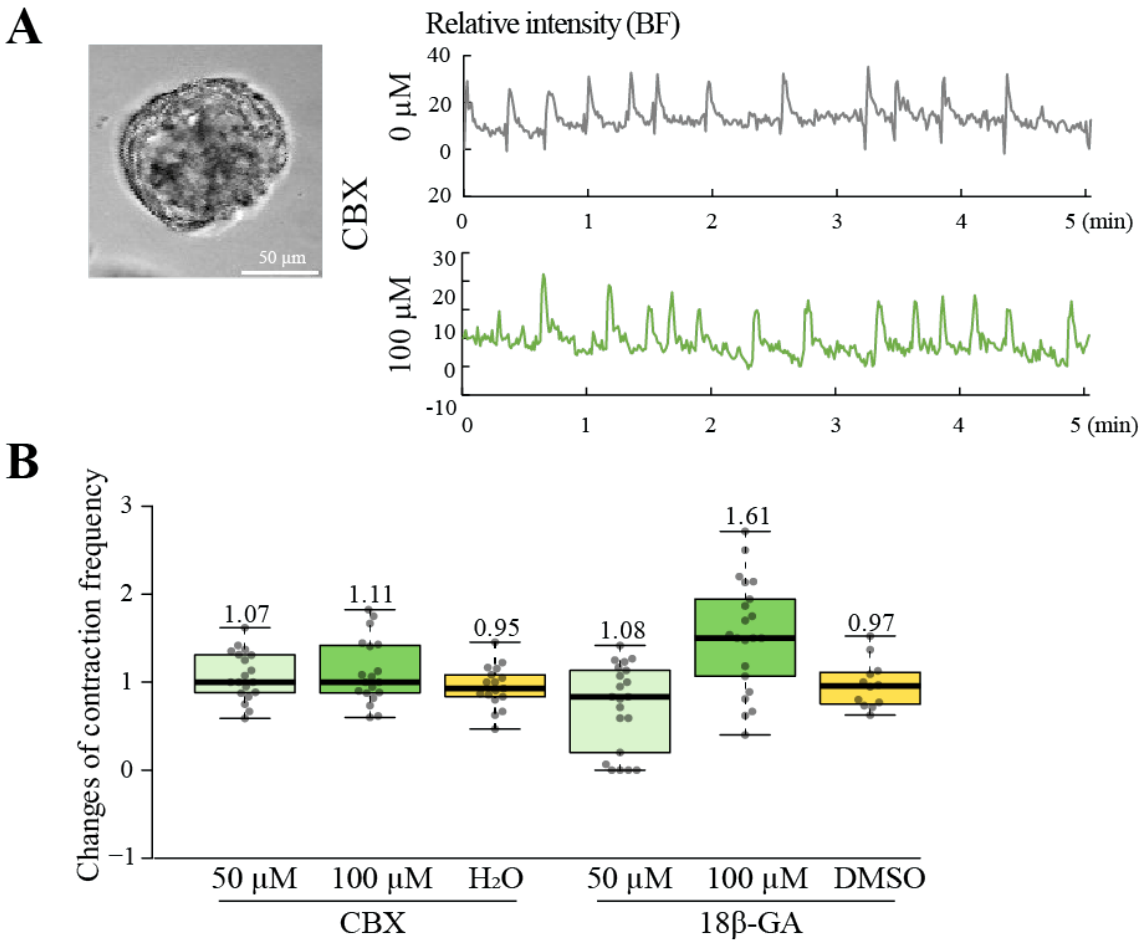

Supplementary Figure S3

(A) Day 7 organoid exhibited periodic contractions both before (0 µM; control) and after adding CBX. Graphs show contractions quantified by the difference in intensity of brightfield in sequential images. (B) Relative changes to the control in contraction frequency in day 7 organoid after CBX. The number is an average. Scale bar: 50 µm in A.

Movie 1

Long-term time-lapse imaging after seeding. Time lapse was taken every 2 hours for a total of 100 hours. This video corresponds to Fig. 1B.

Movie 2

Periodic contractions of the cluster/spheroid on day 3, 5 and 7. Time-lapse images were taken with 700 msec intervals for 5 min. This video corresponds to Fig. 2A.

Movie 3

Periodic contractions of a day 7 organoid with CBX. Time-lapse images were obtained with 700 msec intervals for 5 min. This video corresponds to Fig. S3.

Movie 4

Ca^{2+} dynamics in day 7 gut contractile organoid are concomitant with its contractions. Time-lapse images were obtained with 700 msec intervals for 5 min. This video corresponds to Fig. 4.

Movie 5

Ca^{2+} dynamics in a gut contractile organoid with CBX. Time-lapse images were obtained with 700 msec intervals for 5 min. This video corresponds to Fig. 5.

Movie 6

Ca^{2+} dynamics in day 7 gut contractile organoid with Blebbistatin. Time-lapse images were obtained with 700 msec intervals for 5 min. This video corresponds to Fig. 6.

Movie 7

Live imaging during fusion of multiple organoids. Time-lapse images were obtained every 10 minutes for 4 hours. This video corresponds to Fig. 7A.

Movie 8

Ca^{2+} transients in two gut contractile organoids before and after fusion. Time-lapse images were obtained with 450 msec intervals for 5 min. This video corresponds to Fig. 7B.

Movie 9

829 Ca^{2+} transients in three gut contractile organoids in 3-well hydrogel with channels.
830 Time-lapse images were obtained with 700 msec intervals for 5 min. This video
831 corresponds to Fig. 8C.
832
833 **Movie 10**
834 Ca^{2+} transients in three gut contractile organoids in 3-well hydrogel *without*
835 channels. Time-lapse images were obtained with 450 msec intervals for 5 min. This
836 video corresponds to Fig. 8G.
837
838 **Movie 11**
839 Similar assay to movie 10 with 18β-GA administration. Time-lapse images were
840 obtained with 700 msec intervals for 5 min. This video corresponds to Fig. 8H.